buildings

MDPI

Article

Synergistic Effects of Steel Scale Waste and Graphite Nano/Micro Platelets on Concrete Performance

Suniti Suparp [1], Mohsin Ahmad Butt [2], Adnan Nawaz [2,*], Rana Faisal Tufail [2], Shahzadi Irum [2], Preeda Chaimahawan [3,*], Chisanuphong Suthumma [4,*] and Afaq Ahmad [5,6,*]

1 Department of Civil and Environmental Engineering, Faculty of Engineering, Srinakharinwirot University, Nakhonnayok 26120, Thailand; suniti@g.swu.ac.th
2 Department of Civil Engineering, COMSATS University Islamabad, Wah Campus, Wah Cantt 47040, Pakistan; mohsinahmad1997@gmail.com (M.A.B.); faisal.tufail@ciitwah.edu.pk (R.F.T.); irum.jawad@ciitwah.edu.pk (S.I.)
3 School of Engineering, University of Phayao, Phayao 56000, Thailand
4 Department of Civil Engineering, Faculty of Engineering at Kamphaeng Saen, Kasetsart University, Nakhon Pathom 73140, Thailand
5 Department of Civil Engineering, Herff College of Engineering, University of Memphis, Memphis, TN 38152, USA
6 Faculty of Technology, Art and Design, OsloMet University, 0176 Oslo, Norway
* Correspondence: adnan.nawaz@ciitwah.edu.pk (A.N.); preeda.ch@up.ac.th (P.C.); chisanuphong.s@ku.th (C.S.); afaq.ahmad@oslomet.no (A.A.)

Abstract

Sustainable materials are increasingly being incorporated into high-strength concrete (HSC) to reduce environmental impact while maintaining structural performance. This study experimentally investigates the combined use of steel scale waste (SSW) as a replacement for natural fine aggregates and graphite nano/micro platelets (GNMPs) as a nano-modifying additive in HSC. Natural sand was replaced with SSW at levels of 0%, 50%, and 100%, while GNMPs were incorporated at dosages of 0%, 0.1%, 0.3%, and 0.5% by weight of cement. The results indicate that partial replacement of sand with SSW significantly improves concrete density and mechanical performance due to enhanced particle packing and the high specific gravity of steel scale particles. At the nanoscale, GNMPs contribute to pore refinement, improved nucleation of hydration products, and crack-bridging within the cement matrix, thereby strengthening the interfacial transition zone and delaying crack propagation. The combined effect of these mechanisms produces a synergistic enhancement in concrete performance. The optimum mixture containing 50% SSW and 0.3% GNMPs achieved a compressive strength of 68.2 MPa and splitting tensile strength of 7.6 MPa, representing improvements of approximately 54% and 52%, respectively, compared with the control mix. Durability-related properties such as water absorption and sorptivity were also significantly improved due to matrix densification and pore structure refinement. Although the incorporation of SSW and GNMPs reduced workability, all mixtures remained within a practical range for casting. The developed concrete is particularly suitable for structural applications requiring high strength and durability, such as high-rise building components, bridge elements, and precast structural members. The findings demonstrate that the combined use of industrial steel waste and nano-reinforcement offers a promising pathway toward sustainable and high-performance concrete.

Keywords: graphite nano platelets; steel scale waste; fresh properties; hardened properties; concrete; green infrastructure; sustainable development; buildings

Academic Editor: Pavel Reiterman

Received: 8 February 2026
Revised: 20 March 2026
Accepted: 22 March 2026
Published: 26 March 2026

1. Introduction

Concrete is the most widely used material in construction and forms the backbone of modern infrastructure [1,2]. It is preferred because it can be shaped easily, raw materials are readily available, and the overall cost is relatively low [3]. However, the production of concrete is not without concerns [4]. In particular, cement, which acts as the main binding component, requires a large amount of energy to produce. This process releases a considerable amount of greenhouse gases, making concrete production an important environmental issue worldwide [5,6]. It has been reported in the literature that cement production is accountable for nearly 8% of the total anthropogenic CO_2 emissions worldwide [7]. In addition, the concrete industry requires large amounts of natural aggregates and water, which further increases the pressure on already limited natural resources [8,9]. Rapid urbanization and continuous population growth have greatly increased the demand for concrete, specifically in developing countries. As a consequence, excessive extraction of natural river sand has taken place, leading to serious environmental issues such as riverbank erosion, damage to aquatic ecosystems, and depletion of groundwater resources [10]. In Pakistan and other South Asian regions, uncontrolled sand mining has also led to long-term ecological as well as economic problems. These challenges emphasize the urgent need to identify sustainable alternatives to natural fine aggregates while maintaining the required structural performance of concrete. To address these challenges, recent research on sustainable concrete has increasingly focused on the use of industrial by-products and waste materials. The adoption of the 3R approach, namely reduce, reuse, and recycle, has promoted the addition of waste-based materials in concrete production [11]. Previous studies have demonstrated that materials like fly ash [12,13], metakaolin-enhanced laterite rock aggregate concrete, silica fume [14,15], steel slag [16,17], waste glass powder [18,19], and marble waste [20] can partially replace conventional constituents while retaining adequate mechanical and durability properties. These approaches help in lowering environmental impact, conserving natural resources, and at the same time reducing problems related to waste disposal.

The iron and steel industry generates a large amount of industrial solid waste. During steel production, especially in the hot rolling stage, mill scale is formed as a result of surface oxidation. This waste, commonly known as steel scale waste (SSW), mainly contains iron oxides along with small quantities of other metallic compounds such as magnetite and hematite [21]. On average, approximately 10–20 kg of mill scale waste is generated per ton of steel [11]. Because of its relatively high specific gravity and particle size distribution like that of natural sand, SSW has gained attention as a possible substitution for fine aggregate in concrete [22]. Several studies have shown that replacing natural sand partially with steel mill scale can improve concrete density and compressive strength, provided that suitable replacement levels are used [23,24]. This improvement is usually linked to better particle interlocking and higher packing density. However, when the replacement level becomes too high, workability may decrease, and strength can be affected because of poor grading and rough surface texture. Therefore, determining the optimum replacement ratio is still an important research challenge. Alongside waste utilization approaches, nanotechnology has emerged as a promising solution to improve the performance of cement-based products. Nanomaterials, generally characterized by particle sizes smaller than 100 nm, show unique physical and chemical properties when compared to conventional materials [25]. When added to cement-based composites, nanomaterials can help refine the pore structure, speed up hydration reactions, and improve the bonding between the cement paste and aggregates [26,27]. These effects together lead to better mechanical strength and improved durability of concrete. Among the different types of nanomaterials, carbon-based nanomaterials have attracted considerable attention. Graphite nano/micro platelets (GNMPs), which consist of stacked graphene layers, have a two-dimensional platelet shape with a high aspect ratio and a large surface area [28,29]. Compared to carbon nanotubes, GNMPs are relatively economical and easier to disperse when appropriate surfactants are used [30]. Because of their platelet shape, GNMPs can transfer stresses more effectively and help bridge microcracks within the cement matrix, which makes them suitable for use in concrete applications. Many experimental studies have reported that the addition of GNMPs improves the mechanical performance of cement-based composites. Increases in compressive strength, splitting tensile strength, flexural strength, and energy absorption capacity have been linked to the filler effect, crack-arresting behavior, and improvement in the interfacial transition zone (ITZ) [28,31,32]. Previous research has consistently shown that there is an optimum GNMP content, usually around 0.3% by weight of cement, at which maximum performance improvement is achieved. At higher dosages, GNMPs tend to agglomerate, which can reduce strength instead of improving it [33,34]. In addition to mechanical improvements, GNMPs have also shown positive effects on durability-related properties. Studies have reported reduced water absorption, lower sorptivity, and improved resistance to chloride ion penetration, mainly due to matrix densification and refinement of the pore structure [35,36]. These improvements are especially important for high-strength concrete that is exposed to aggressive environments. However, when GNMP content becomes excessive, strong van der Waals forces can cause agglomeration, which negatively affects workability and uniformity of the mix [37,38]. Although SSW and GNMPs have been widely studied on their own, only limited research is available on their combined use in high-strength concrete. The interaction between dense steel scale particles and nano-sized graphite platelets may offer additional benefits. These may include better particle packing, improved crack resistance, and enhanced durability performance [39]. High-strength concrete (HSC), normally referred to as the concrete with compressive strength exceeding 55 MPa, roughly, provides an ideal matrix to study such interactions because of its dense microstructure and low water-to-binder ratio [40,41]. Moreover, earlier studies have emphasized that modification of the interfacial transition zone, improvement in particle packing density, and refinement of the microstructure are key factors in achieving high-performance concrete [42]. The combined use of industrial waste materials together with nanomaterials fits well with the goals of sustainable construction and has been identified as a promising direction for future research in concrete engineering [43,44]. Therefore, this study focuses on experimentally examining the synergetic effect of SSW and graphite nano/micro platelets on the mechanical and durability behavior of high-strength concrete.

In this work, SSW is used as a partial and full substitution of natural fine aggregates, while GNMPs are added at different dosage levels as a nano-reinforcing material. The aim is to obtain suitable material dosages at which an optimum concrete performance is obtained, in addition to enhanced durability. This study is a contribution to the field of sustainable construction, as the synergistic effects of SSW and GNMPs are investigated as innovative materials for high-strength concrete. The novelty of the work is the dual approach of the use of SSW as a partial replacement of natural fine aggregates and the introduction of GNMPs as a nano-modifying admixture with the aim of addressing environmental sustainability and mechanical performance. The results show that a 50% substitution of natural fine aggregates with SSW with a dosage of 0.3% of GNMPs gives significant improvements in compressive and tensile strengths, thereby representing an advancement for the use of industrial by-products in concrete formulations. In addition, the research highlights the tradeoff between workability and strength, providing insights on how to optimise concrete mixtures for practical use. Nanomaterials such as graphene nanoplatelets and graphite nano/micro platelets tend to agglomerate due to strong van der Waals forces and their hydrophobic nature, which significantly reduces their effectiveness in cementitious

https://doi.org/10.3390/buildings16071315

composites. Therefore, achieving uniform dispersion is essential to fully utilize their reinforcing potential. Various dispersion techniques have been proposed in the literature, including the use of chemical surfactants, polymer dispersants, high-shear mixing, and ultrasonication. Among these approaches, the use of natural surfactants such as acacia gum has gained attention due to its ability to adsorb onto graphitic particle surfaces, weaken intermolecular attractions, and stabilize nanoparticle suspensions in aqueous environments while maintaining compatibility with cement systems [45–48].

Despite the growing interest in sustainable concrete materials, several important research gaps remain. Previous studies have examined the use of SSW as a partial replacement for natural aggregates to reduce industrial waste and improve resource efficiency. Similarly, graphene-based or GNMPs have been widely investigated as nano-reinforcements capable of enhancing the mechanical and durability properties of cementitious composites through crack-bridging, nucleation of hydration products, and pore refinement. However, most existing studies have investigated these materials independently, and the combined or synergistic interaction between industrial steel waste particles and nano-reinforcing platelets in high-strength concrete has not been systematically explored. Recent studies on sustainable concrete materials [49] have shown that modifying the cement matrix using supplementary materials can significantly improve microstructural densification and mechanical performance of alternative aggregate concretes. However, the potential for simultaneously incorporating industrial steel waste aggregates and nano-reinforcing carbon-based materials to achieve both sustainability and performance enhancement remains insufficiently investigated. Therefore, the present study aims to address this gap by systematically evaluating the synergistic effects of SSW and GNMPs on the mechanical properties and durability indicators of high-strength concrete, while also identifying optimal replacement levels for practical structural applications.

2. Design of Experiments

2.1. Test Matrix

The experimental program was designed to examine the synergetic impact of SSW and GNMPs on the mechanical and durability response of high-strength concrete. A total of twelve concrete mixes were produced by varying two primary parameters: the replacement level of natural fine aggregate with SSW and the dosage of GNMPs by weight of cement. Natural sand was replaced with SSW at three levels (0%, 50%, and 100%), while GNMPs were incorporated at four dosages (0%, 0.1%, 0.3%, and 0.5%). This matrix allowed both the individual and synergistic effects of SSW and GNMPs to be examined systematically. All concrete mixes were proportioned to achieve a target compressive strength of 50 MPa corresponding to high-strength concrete, while maintaining a constant water-to-cement ratio of 0.30 across all mixtures. The cement content was kept uniform for all mixes, and silica fume and quartz powder were incorporated as supplementary materials to improve particle packing and matrix densification. The replacement of fine aggregates was carried out on a volumetric basis to ensure consistency in grading, while GNMPs were added as a percentage of cement mass. HSC cylinders with dimensions of 100 mm × 200 mm were cast using a mix proportion of (cement:sand/SSW:coarse aggregate) equal to 1:1.5:2.5. The mixtures involved partial to full replacement of natural sand with SSW, along with different addition levels of GNMPs. To achieve high-strength concrete, silica fume, quartz powder, and Viscocrete-3110 superplasticizer were also included based on the weight of cement. This study used a total water-to-binder ratio of 0.30, accounting for cement and all supplementary binders. The details of the sample designation methodology and concrete mix design are given in Tables 1 and 2, respectively. The study targets high-strength concrete (>40 MPa), which necessitates a high binder content to achieve the required microstructure and durability. A cement content of 700 kg/m^3 was therefore used to ensure target strength and to meaningfully assess the effects of SSW and GNMPs.

Table 1. Sample designation methodology.

S. NO.	MIX Design Designation	Sand: Steel Scale Waste	GNMPs
1	G0-SSW0	100:0	0%
2	G0.1-SSW0	100:0	0.1%
3	G0.3-SSW0	100:0	0.3%
4	G0.5-SSW0	100:0	0.5%
5	G0-SSW50	50:50	0%
6	G0.1-SSW50	50:50	0.1%
7	G0.3-SSW50	50:50	0.3%
8	G0.5-SSW50	50:50	0.5%
9	G0-SSW100	0:100	0%
10	G0.1-SSW100	0:100	0.1%
11	G0.3-SSW100	0:100	0.3%
12	G0.5-SSW100	0:100	0.5%

Table 2. Mix design of casting.

No.	Cement (Kg/m^3)	F.A (Kg/m^3)	SSW (Kg/m^3)	C.A (Kg/m^3)	GNMPs (Kg/m^3)	S.F (Kg/m^3)	QZ (Kg/m^3)	SP (Kg/m^3)	Water (Kg/m^3)
1	700	1050	0	1750	0	70	280	14	210
2	700	1050	0	1750	0.7	70	280	14	210
3	700	1050	0	1750	2.1	70	280	14	210
4	700	1050	0	1750	3.5	70	280	14	210
5	700	525	525	1750	0	70	280	14	210
6	700	525	525	1750	0.7	70	280	14	210
7	700	525	525	1750	2.1	70	280	14	210
8	700	525	525	1750	3.5	70	280	14	210
9	700	0	1050	1750	0	70	280	14	210
10	700	0	1050	1750	0.7	70	280	14	210
11	700	0	1050	1750	2.1	70	280	14	210
12	700	0	1050	1750	3.5	70	280	14	210

Note: F.A is fine aggregates, SSW is steel scale waste, C.A is coarse aggregates, S.F is silica fume, QZ is quartz powder, and SP is superplasticizer.

2.2. Material Properties

2.2.1. Cement

Ordinary Portland Type I cement was employed as the main binding material in all concrete mixtures. The employed cement complied with ASTM C150 [50]. The cement was used in its original form without any modification and was stored in dry conditions before mixing. It served as the primary source of strength in the high-strength concrete and was used consistently in all mixes to allow proper comparison of the results. The cement reportedly had a specific gravity of 3.15, and its chemical composition was as given by the manufacturer. A typical sample is illustrated in Figure 1a. Recent assessments indicate that the studied SSW is not classified as hazardous and is widely reused in ironmaking, for example, as a feedstock in pig iron production [51,52]. Nevertheless, its large annual generation—typically 10–20 kg per tonne of steel—creates substantial logistical, economic, and environmental challenges for steel plants and downstream processors. This study is motivated by the need to evaluate alternative valorization pathways and processing strategies that improve resource efficiency, reduce disposal costs, and expand marketable applications for SSW beyond conventional recycling routes. Addressing these aims supports circular-economy objectives while ensuring safe, cost-effective management of this abundant industrial byproduct.

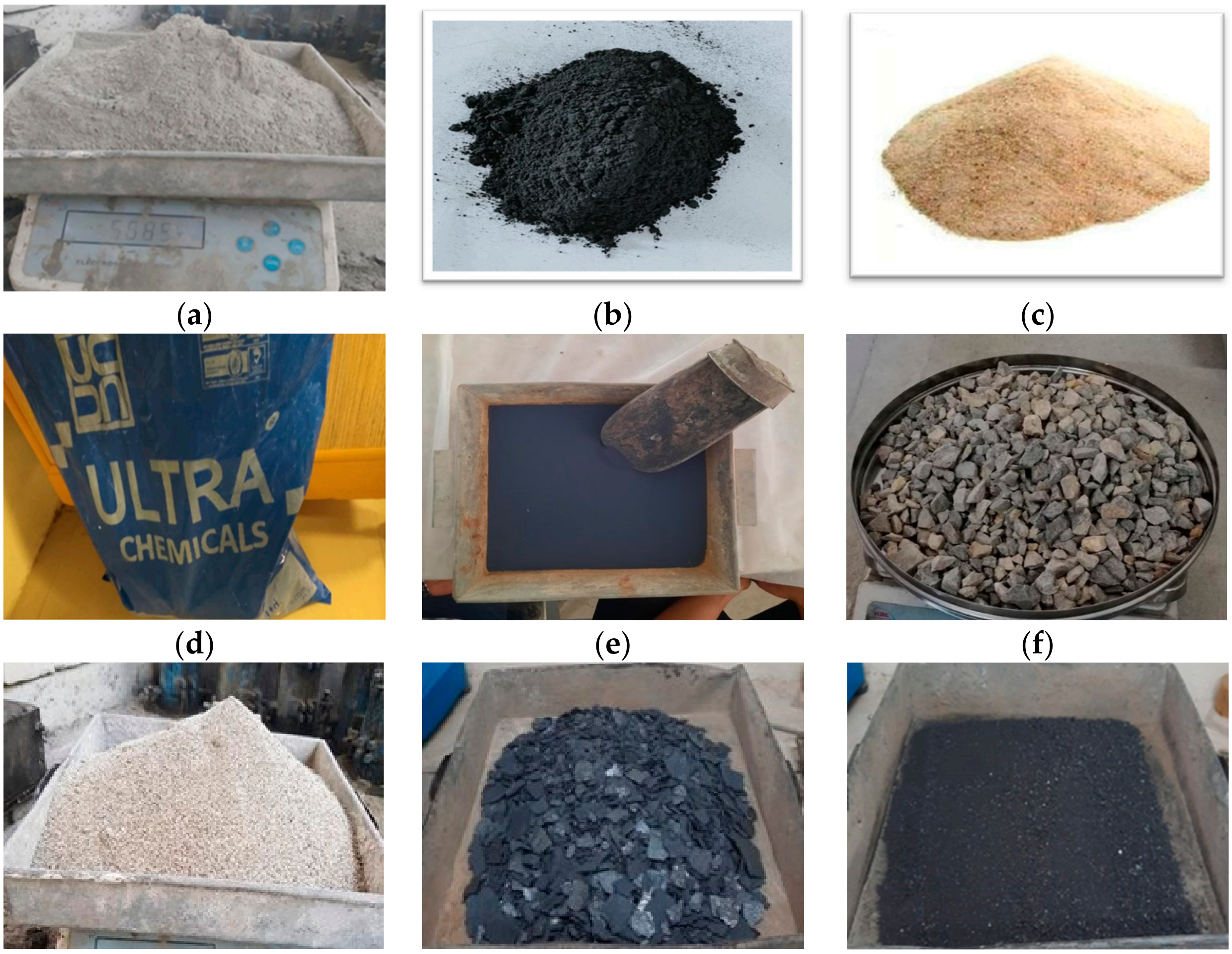

(**g**) (**h**) (**i**)

Figure 1. Materials used: (**a**) cement, (**b**) GNMPs, (**c**) acacia gum, (**d**) quartz powder, (**e**) silica fume, (**f**) coarse aggregates, (**g**) natural fine aggregates, (**h**) flaky SSW, and (**i**) crushed SSW.

2.2.2. Graphite Nano Micro Platelets

GNMPs are carbon-based conductive nanoparticles that originate from natural graphite, a layered material consisting of stacked, parallel 2D graphene layers. The architectural features of GNMPs, namely, their two-dimensional configuration, nanoscale thickness, and submicron to 100 µm diameters, confer exceptional mechanical and electrical properties. Specifically, GNMPs' high aspect ratio and large surface area enable efficient reinforcement and conductive networking in cementitious materials at minimal concentrations, thereby surpassing the performance of conventional carbon-based fillers, including carbon fibers, graphene, and carbon black. Figure 1b shows a typical GNMPs sample. The density, specific gravity, and surface area of GNMPs were 2.18 g/cm^3, 1.91, and 24 m^2/g, respectively.

2.2.3. Acacia Gum

Acacia gum was used as a natural surfactant to facilitate the dispersion of GNMPs in the aqueous medium. GNMPs have a strong tendency to agglomerate due to their large specific surface area and the presence of strong van der Waals forces between individual platelets. The addition of acacia gum helps to overcome this limitation by adsorbing onto the surface of GNMP particles and converting their hydrophobic surface into a hydrophilic one, thereby improving dispersion stability in water [49]. In the present study, the dispersion process involved mixing GNMPs with an acacia gum solution, followed by mechanical ultrasonication for approximately 45 min to achieve a homogeneous suspension. The surfactant-to-GNMP ratio was selected based on previous experimental investigations, where an optimum ratio of approximately 0.6:1 (AG:GNMP) was found to provide stable dispersion and maximum absorbance values in UV–Vis spectroscopy measurements [34]. A pictorial view of acacia gum is presented in Figure 1c. Compared with other dispersion techniques such as synthetic surfactants, polymer dispersants, or high-speed shear mixing, the acacia gum–ultrasonication approach provides several advantages, including improved environmental compatibility, reduced chemical interference with cement hydration, and effective stabilization of nanoparticle suspensions. Consequently, this method was adopted to ensure reliable dispersion of GNMPs within the concrete matrix.

2.2.4. Quartz Powder

Quartz powder as a filler plays an important role in high-strength concrete (HSC) by reducing the initial voids in the mixture, which ultimately contributes to higher strength development. Quartz is a commonly available mineral found in various geological environments and was incorporated into the concrete mix at 40% of the cement content. The quartz powder employed in this study was procured from Ultra Chemicals, as illustrated in Figure 1d.

2.2.5. Silica Fume

The addition of silica fume, due to its very fine particle size, improves the workability of concrete by allowing a reduction in the water-to-cement ratio, especially when used together with superplasticizers. Silica fume is considered an essential component in the production of HSC and was therefore incorporated in all mixes of this study. Silica fume was included at a dosage of 10% of the cement content. As provided by the manufacturer, the SiO_2 content, surface area, moisture content, and bulk density of silica fume were >85%, 15,000–30,000 m^2/kg, <3%, and 600–750/m^3, respectively. A pictorial view of silica fume is presented in Figure 1e.

2.2.6. Coarse Aggregates

The coarse aggregates in this study are sourced from Taxila crushing plants, comprising a downgrade of 12.5mm and the following fractions: 12.5 mm, 9.5 mm, and 4.75 mm. To ensure compliance with ASTM C33 [53], the aggregates underwent thorough cleaning, drying to achieve a saturated surface dry condition, and controlled watering. The fineness modulus, specific gravity, water absorption, and bulk density were 2.86, 2.62, 0.82%, and 1582 kg/m^3, respectively. A pictorial view of coarse aggregates is presented in Figure 1f.

2.2.7. Natural Fine Aggregates

The fine aggregate (sand) was obtained from a borrow pit located in Lawrancepur, Pakistan. Before use, the sand was passed through a #4 sieve to eliminate oversized particles and to ensure a more uniform gradation. The sand was dried prior to mixing, and appropriate moisture content corrections were applied during batching. The fineness modulus, specific gravity, and water absorption were 2.61, 2.73, and 1.7%, respectively. A pictorial view of natural fine aggregates is presented in Figure 1g.

2.2.8. Steel Scale Waste

This study employed Steel Scale Waste, commonly referred to as mill scale, which was collected from local re-rolling mills located in the Hattar Industrial Estate, Pakistan. The

https://doi.org/10.3390/buildings16071315

material appeared as a black powdered substance with particle sizes generally comparable to those of natural sand. Due to its comparatively higher specific gravity and lower water absorption in comparison to ordinary sand, mill scale presents potential as an alternative fine aggregate in HSC, with possible improvements in density and workability. For this investigation, the mill scale was separated into three different grades through a screening process. Grade I consisted of particles in the range of 2–1.18 mm, Grade II ranged from 1.18 mm to 0.6 mm, and Grade III included particles between 0.6 mm and 0.075 mm. Packing density tests were carried out for unitary, binary, and ternary combinations of these grades in order to identify the most suitable mix composition. The mill scale collected from the steel mills initially consisted of irregular, flat flakes (see Figure 1h) with lengths in the range of 25 mm to 50 mm. In order to make its size comparable to that of natural sand, the mill scale was crushed into smaller particles using a Los Angeles abrasion machine before being used in the concrete mixes (see Figure 1i). The specific gravity of SSW was 4.50. Although the present study adopted a combined gradation approach to replicate the grading characteristics of natural sand, the influence of individual gradations and optimized composite gradations of SSW on concrete performance was not investigated in detail. Future research could explore gradation optimization strategies to further enhance packing density, mechanical performance, and durability of SSW-based high-strength concrete.

2.2.9. Superplasticizer

The high-performance superplasticizer Viscocrete-3110 was used to enhance the overall properties of the concrete. Viscocrete-3110 helps in reducing the water content by approximately 20–30%, which supports improved workability, strength development, and durability of the concrete. It also does not cause any harmful effects on the concrete matrix or steel reinforcement.

2.2.10. Tap Water

In order to maintain experimental simplicity and accessibility, this study employed normal tap water from the laboratory as its water source.

2.3. Casting and Curing of Specimens

This study followed standard casting and curing procedures in accordance with ASTM C192/C192M [54] to ensure consistency and reliability of the experimental results. All specimens were cast in the laboratory in controlled environmental settings, with a temperature of 20 °C ± 2 °C and relative humidity of 60% ± 10%. After casting, the specimens were demolded after 24 h. The curing was then conducted by dipping the specimens in water maintained at a constant temperature of 23 °C ± 2 °C, which was carefully controlled to support proper cement hydration, strength gain, and microstructural development. The pan-type mixer was employed for concrete mixing. Mechanical vibration using a laboratory vibration table was applied during casting to ensure full consolidation.

2.4. Testing Methods

After completion of the curing period, a comprehensive testing program was conducted to evaluate the mechanical performance and durability of the different mix designs. The testing scheme was divided into two main categories. Destructive testing (DT) was carried out to assess ultimate strength, failure modes, and stress–strain response of the specimens. In addition, non-destructive testing (NDT) was performed to monitor structural integrity, cracking behavior, and possible degradation. The details of the testing methods, procedures, and evaluation criteria are summarized in Table 3, providing a complete understanding of the behavior of the specimens under various loading conditions.

Table 3. Details of test methods adopted and related standards.

Serial No.	Description	ASTM Standards
	Destructive testing	
1	Standard Test Procedure for Cylindrical Concrete Specimens' Compressive Strength	C-39 [55]
2	Standard Test Procedure for Splitting Tensile Strength of Concrete Specimens in Cylindrical Form	C-496 [56]
	Non-destructive testing	
3	Slump Test	C143 [57]
4	Water Absorption Test	C642 [58]
5	Dry Density Test	C596 [59]
6	Bulk Water Sorptivity Test	C1585 [60]
7	Ultra Sonic Pulse Velocity Test	C597 [61]
8	Chloride Ion Penetration Test	C1202 [62]

2.4.1. Compressive Strength Test

The compressive strength was obtained by following the steps in ASTM C39 [55] using a 1000 kN universal testing machine. Cylindrical samples with dimensions of 100 mm × 200 mm were employed after 28 days of curing. As illustrated in Figure 2a, the load was imposed at a constant rate of 0.20 MPa/s without any shock loading until failure of the specimens, following the prescribed testing procedure.

(a) (b) (c) (d)

Figure 2. *Cont.*

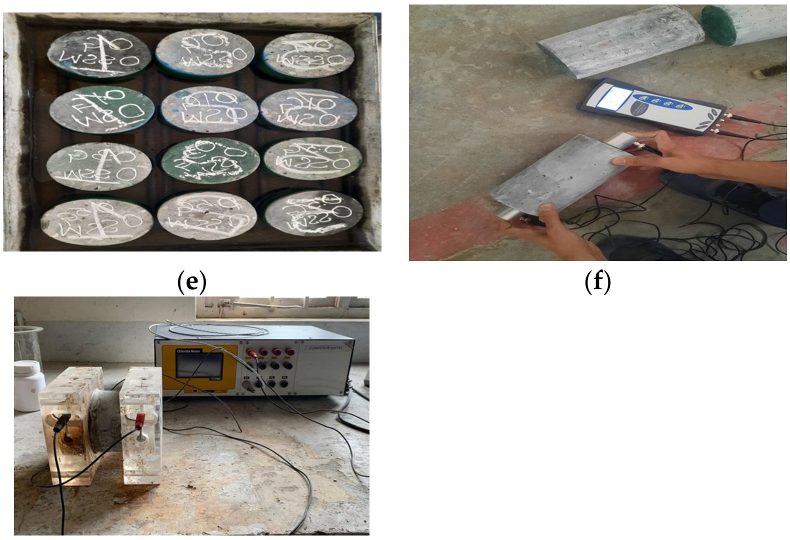

(**e**) (**f**) (**g**)

Figure 2. Testing methods: (**a**) compression test, (**b**) splitting tensile test, (**c**) slump test, (**d**) water absorption test, (**e**) Bulk water sorptivity test, (**f**) UPV test, and (**g**) rapid chloride ion test.

2.4.2. Splitting Tensile Test

This test was conducted as an indirect approach to evaluate the tensile strength of concrete using the splitting tensile strength method in accordance with ASTM C-496 [56]. Cylindrical samples with dimensions of 100 mm × 200 mm were employed after 28 days of curing. As illustrated in Figure 2b, the load was applied at a constant rate of 0.25 MPa/s until the sample failed.

2.4.3. Slump Test

The slump test was conducted in accordance with ASTM C143 [57] to evaluate the workability and consistency of fresh hydraulic-cement concrete. The procedure involved cleaning and moistening the slump cone and base plate, placing the cone on a level surface, and filling it with a representative concrete sample in 3 equal layers. Each layer was compacted using 25 uniform strokes. After the cone was completely filled, it was lifted vertically for the concrete to slump. The change between the initial height of the cone and the highest point of the dropped-down concrete was then determined. As shown in Figure 2c, this number provides an indication of the consistency and workability of the concrete, where timely execution and careful measurement are essential to obtain reliable results.

2.4.4. Water Absorption Test

To determine the water absorption percentage of cylindrical concrete samples with dimensions of 100 mm × 200 mm, the water absorption test was employed in accordance with ASTM C642 [58]. The specimens were oven-dried at 105 °C for one day and then allowed to cool to a temperature range of 20–25 °C, after which their dry mass (A) was recorded. The samples were subsequently immersed in water for a duration of 48 h. A pictorial representation of the test setup is shown in Figure 2d. After removal and surface-drying, the mass (B) was recorded. The water absorption percentage was calculated using Equation (1):

$$Water\ absorption\ (\%) = \left[\frac{B-A}{A}\right] \times 100 \quad (1)$$

2.4.5. Dry Density Test

The dry density of the concrete specimens was determined at 28 days to examine the influence of different materials on density. Cylindrical samples with dimensions of 100 mm × 200 mm were weighed, and the dry density was determined using the determined mass and the corresponding volume of each sample.

2.4.6. Bulk Water Sorptivity Test

The bulk water sorption test was performed to evaluate the durability of concrete specimens under wetting and drying situations in accordance with ASTM C1585 [60]. This test quantified the amount of water absorbed by the bulk mass of dried and hardened concrete samples when submerged in water. The specimens were immersed for a total duration of 48 h, and their weights were recorded at time intervals of 1, 5, 10, 15, and 30 min, followed by measurements at 24 h and 48 h. Cylindrical samples with 100 mm diameter and 50 mm height were oven-dried at 50 °C for 48 h until a constant mass was achieved. After drying, the samples were placed in sealed containers for one day, and the oven-dried mass of each sample was calculated. Then, the specimens were submerged in water maintained at a temperature of 23 ± 3 °C, with the water level kept at 25 ± 10 mm. At each specified interval, the specimens were taken out of the water, and extra surface water was smoothly removed utilizing an absorbent cloth before recording the mass. The bulk water sorption was calculated using Equation (2):

$$Bulk\ Water\ Sorption\ (\text{mm}) = \frac{(W - D)}{(A \times d)} \tag{2}$$

where W is the mass of the submerged specimen (g), D is the oven-dried mass of the specimen (g), A is the surface area of the specimen (mm^2), and d is the density of water taken as 0.001 g/mm^3. The surface area of the specimen was calculated using Equation (3):

$$A = 3.14 \times sd \times \left(\frac{sd}{2} + h\right) \tag{3}$$

where sd is the diameter of the specimen (mm), and h is the height of the specimen (mm). Figure 2e illustrates the experimental setup adopted for the bulk water sorption test.

2.4.7. Ultrasonic Pulse Velocity Test

The ultrasonic pulse velocity (UPV) test was carried out in accordance with ASTM C597 [61] to evaluate the internal quality and uniformity of the concrete specimens. In this test, ultrasonic transducers were placed on opposite faces of the concrete cylinders, allowing a pulse to be transmitted through the specimen while the travel time was recorded. The pulse velocity was determined by dividing the distance between the transducers by the measured travel time. Generally, higher pulse velocities indicate dense and good-quality concrete with fewer internal defects, whereas lower values may point to the presence of cracks, voids, or other imperfections. Owing to its non-destructive nature, the UPV test is useful for quality control and assessment of concrete condition, as illustrated in Figure 2f.

2.4.8. Rapid Chloride Ion Test

The endurance of concrete against chloride ion penetration was assessed using a test procedure similar to ASTM C1202 [62]. In this method, concrete cylindrical specimens were exposed to a chemical solution for a specified duration. The chloride ion penetration endurance was evaluated based on the total electrical charge passed through the specimen, expressed in Coulombs (C). A schematic look of the test setup adopted in this study is illustrated in Figure 2g.

https://doi.org/10.3390/buildings16071315

3. Experimental Results

3.1. Compressive Strength

The compressive strength findings of high-strength concrete incorporating SSW and GNMPs are presented and discussed in this section. All specimens were tested after 28 days of water curing, and the results are compared with the control mix containing natural sand and no GNMPs. The influence of both SSW replacement level and GNMP dosage on compressive strength was clearly observed, indicating a combined effect of particle packing and nano-scale reinforcement. For concrete mixes without GNMPs, partial substitution of natural sand with SSW led to an improvement in compressive strength up to the 50% substitution level (see Figure 3 and Table 4). This improvement can be ascribed to the greater specific gravity of SSW and improved packing density, which resulted in a denser concrete matrix. However, when natural sand was fully substituted with SSW, a reduction in compressive strength was observed. This strength loss is likely associated with reduced workability and non-uniform particle distribution, which may have introduced localized voids despite the dense nature of the steel scale particles. The 28-day compressive strength results presented in Table 4 show a clear influence of both SSW replacement level and GNMP content on concrete performance. The control mix containing natural sand and no GNMPs (G0-SSW0) achieved an average compressive strength of 44.3 MPa. The incorporation of GNMPs at 0.1% and 0.3% increased the compressive strength to 48.5 MPa and 52.6 MPa, corresponding to improvements of approximately 9.5% and 18.7%, respectively. However, increasing the GNMP dosage to 0.5% did not result in further improvement, and the strength remained at 48.5 MPa, indicating a decline beyond the optimum GNMP content.

For concrete mixes with 50% substitution of natural sand by SSW, a significant enhancement in compressive strength was noted even in the absence of GNMPs. The reference mix (G0-SSW50) achieved an average compressive strength of 57.7 MPa, showing a 30.3% increase over the control mix. With the addition of GNMPs, further strength gains were recorded, reaching 62.4 MPa and 68.2 MPa at 0.1% and 0.3% GNMPs, respectively. The maximum compressive strength of 68.2 MPa corresponds to an overall increase of approximately 54.0% relative to the control mix, highlighting a pronounced synergistic effect between optimized SSW content and nano-scale reinforcement. At 0.5% GNMPs, the compressive strength decreased to 58.5 MPa, although it remained 32.1% greater than the control mix. When natural sand was fully substituted with SSW (100% SSW), the compressive strength of the mix without GNMPs was 52.0 MPa, which is 17.4% higher than the control mix but lower than the corresponding 50% SSW mixture. The inclusion of GNMPs improved the compressive strength to 56.3 MPa and 62.0 MPa at 0.1% and 0.3%, corresponding to increases of 8.3% and 19.2% relative to the G0-SSW100 mix. A reduction in strength was again observed at 0.5% GNMPs, with an average value of 53.9 MPa. Across all SSW replacement levels, mixes containing 0.3% GNMPs consistently exhibited the highest compressive strength, while the relatively small scatter among individual test results indicates good repeatability and reliability of the experimental data. Although the incorporation of GNMPs generally improves compressive strength at lower dosages, a decline in strength was observed when the GNMP content reached 0.5%. This reduction can be attributed to the tendency of nano-platelet particles to agglomerate at higher concentrations due to strong van der Waals attractions between adjacent layers. Such agglomeration leads to the formation of localized clusters within the cementitious matrix, which act as weak zones and interrupt the uniform distribution of hydration products. These clusters may also increase local porosity and hinder effective stress transfer within the matrix. Consequently, the beneficial effects of GNMPs, such as crack-bridging and nucleation of hydration products, become less effective when the dispersion of nanoplatelets is compromised.

https://doi.org/10.3390/buildings16071315

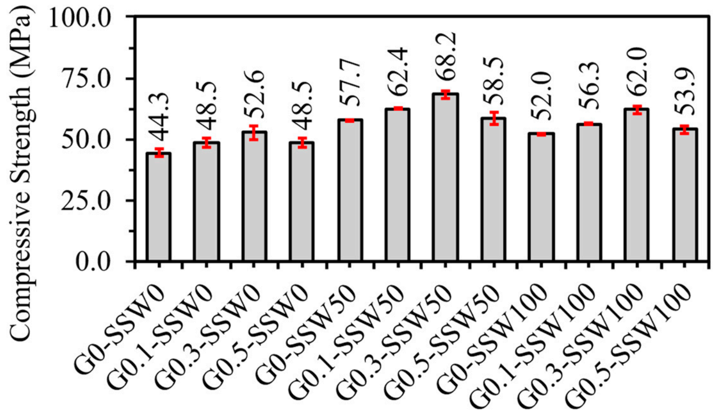

Figure 3. Measured compressive strength of samples.

Table 4. Summary of compressive strength, splitting tensile strength, and slump.

Sample ID	Mean Compressive Strength (MPa)	Standard Deviation	Coefficient of Variation	Mean Splitting Strength (MPa)	Standard Deviation	Coefficient of Variation	Slump (mm)
G0-SSW0	45.27	3.99	1.2%	4.98	1.69	2.3%	110
G0.1-SSW0	49.37	5.41	6.2%	5.43	2.64	6.5%	103
G0.3-SSW0	53.87	6.65	4.5%	5.93	1.35	4.9%	100
G0.5-SSW0	49.23	4.21	9.8%	5.42	3.65	6.3%	97
G0-SSW50	57.72	6.21	7.1%	6.35	4.65	2.1%	94
G0.1-SSW50	61.97	5.69	6.9%	6.82	1.65	3.3%	87
G0.3-SSW50	69.06	6.78	1.2%	7.60	6.25	2.3%	81
G0.5-SSW50	60.10	6.98	3.6%	6.61	1.68	6.4%	79
G0-SSW100	52.03	1.36	1.5%	5.72	2.36	2.3%	66
G0.1-SSW100	56.29	3.98	1.6%	6.19	1.36	6.1%	62
G0.3-SSW100	62.92	4.65	6.1%	6.92	3.21	4.6%	59
G0.5-SSW100	55.00	6.98	1.7%	6.05	1.21	4.5%	57

Across the mixes, the reported error-bar values show that SSW50 consistently has the largest error magnitudes, peaking at G0.3–SSW50 (68.2) and remaining high across G levels (57.7–68.2), suggesting greater variability or uncertainty when SSW is 50%. SSW0 exhibits moderate, relatively uniform error bars (44.3–52.6), indicating steadier performance. SSW100 is highly inconsistent: very low error at G0 (25.0) and G0.3 (32.0) but much larger at G0.1 and G0.5 (56.3 and 53.9), implying SSW100 produces mixed reliability depending on G. In summary, SSW50 yields the largest uncertainties, SSW0 the most consistent, and SSW100 the most variable across G.

3.2. Splitting Tensile Strength

The splitting tensile strength findings demonstrate results like those noted for compressive strength, with clear dependence on both GNMP content and SSW replacement level (see Table 4 and Figure 4). The control mix containing natural sand and no GNMPs (G0-SSW0) exhibited a mean splitting tensile strength of 5.0 MPa. The incorporation of GNMPs led to noticeable improvements, with tensile strength increasing to 5.4 MPa and 5.9 MPa at 0.1% and 0.3% GNMPs, corresponding to increases of approximately 8.0% and 18.0%, respectively. A reduction was observed at 0.5% GNMPs, where the tensile strength remained at 5.4 MPa, indicating that excessive GNMP content does not further enhance tensile performance. For concrete mixes incorporating 50% SSW, a significant enhancement in splitting tensile strength was recorded even in the absence of GNMPs. The reference mix (G0-SSW50) achieved an average tensile strength of 6.4 MPa, representing a 28.0% increase compared to the control mix. With the addition of GNMPs, further improvements were observed, with tensile strength increasing to 6.8 MPa and 7.6 MPa at 0.1% and 0.3% GNMPs, respectively. The highest tensile strength of 7.6 MPa corresponds to an overall improvement of approximately 52.0% relative to the control mix, highlighting a strong synergistic effect between partial SSW replacement and nano-scale reinforcement. At 0.5% GNMPs, the tensile strength decreased to 6.6 MPa, although this value remained 32.0% higher than that of the control mix.

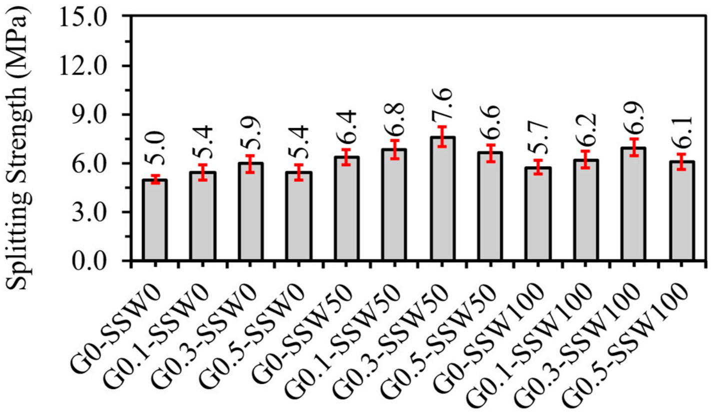

Figure 4. Splitting tensile strength of specimens.

For concrete mixes with 100% substitution of natural sand by SSW, the splitting tensile strength without GNMPs was 5.7 MPa, which is 14.0% greater than the control mix but lower than the corresponding 50% SSW mixture. The inclusion of GNMPs improved the tensile strength to 6.2 MPa and 6.9 MPa at 0.1% and 0.3%, representing increases of 8.8% and 21.1%, respectively, relative to the G0-SSW100 mix. A reduction in tensile strength was again observed at 0.5% GNMPs, with an average value of 6.1 MPa. Overall, mixes containing 0.3% GNMPs consistently achieved the highest splitting tensile strength across all SSW replacement levels, which can be attributed to improved crack-bridging capacity and enhanced interfacial bonding inside the cementitious matrix. A similar trend was observed in the splitting tensile strength results. While moderate GNMP contents improved tensile performance due to enhanced crack-bridging and improved matrix densification, excessive GNMP addition (0.5%) resulted in strength reduction. This behavior can be attributed to the agglomeration of nanoplatelets at higher dosages, which creates localized defects and weak interfacial regions within the cement matrix, thereby reducing the efficiency of stress transfer and crack-arresting mechanisms. Across the mixes, the reported error-bar magnitudes increase with SSW up to 50% and then mostly decrease at 100%. SSW50 shows the largest errors across all G levels (6.4–7.6), with the peak at G0.3–SSW50 (7.6), indicating the greatest uncertainty when SSW = 50%. SSW0 gives the smallest and most uniform errors (5.0–5.9), suggesting the most consistent measurements. SSW100 errors lie between the other two SSW levels (5.7–6.9) and are fairly consistent across G. Overall, SSW50 produces the highest uncertainty, SSW0 the lowest, and SSW100 moderate and stable error magnitudes across G content.

3.3. Slump

The slump test findings indicate a systematic decrease in workability with increasing GNMP content and SSW replacement level (see Table 4). The control mix containing natural sand and no GNMPs (G0-SSW0) exhibited the highest slump value of 110 mm, reflecting adequate workability for high-strength concrete. The incorporation of GNMPs resulted in a gradual reduction in slump to 103 mm, 100 mm, and 97 mm at 0.1%, 0.3%, and 0.5% GNMPs, respectively. This corresponds to a maximum reduction of approximately 12% related to the control mix, even without the inclusion of SSW. The reduction in workability with GNMP addition can be ascribed to the extremely high specific surface area and platelet morphology of graphite nano/micro platelets. GNMPs tend to absorb free water and increase internal friction within the fresh concrete matrix, thereby reducing flowability. Similar reductions in slump have been reported in cementitious systems incorporating carbon-based nanomaterials such as graphene nanoplatelets and carbon nanotubes, where water demand increases significantly due to surface adsorption and particle agglomeration tendencies [30,31]. At higher GNMP dosages, partial agglomeration may further restrict particle mobility, contributing to reduced slump despite a constant water-to-cement ratio.

A more pronounced reduction in slump was observed with increasing SSW content. For mixes without GNMPs, replacing 50% of natural sand with SSW reduced the slump from 110 mm to 94 mm, representing a 14.5% decrease, while full replacement (100% SSW) resulted in a slump of 66 mm, corresponding to an overall reduction of 40%. This behavior is primarily associated with the angular shape, rough surface texture, and higher specific gravity of steel scale particles, which increase inter-particle friction and reduce the lubricating effect provided by natural sand. Similar trends have been produced in earlier works investigating steel-related industrial wastes as fine aggregate replacements. When GNMPs were incorporated into SSW-containing mixes, the combined effect further reduced workability. For the 50% SSW series, slump values decreased from 94 mm to 87 mm, 81 mm, and 79 mm as GNMP content increased from 0% to 0.5%, resulting in an overall reduction of approximately 16% within this group. A similar trend was observed for the 100% SSW mixes, where slump values declined from 66 mm to 57 mm with increasing GNMP dosage. The lowest slump recorded (57 mm) corresponds to the mix containing 100% SSW and 0.5% GNMPs, indicating the combined influence of high surface roughness and nano-scale water adsorption. The observed workability loss in mixes containing both SSW and GNMPs is therefore attributed to the combined effects of increased surface roughness, higher internal friction, and reduced free water availability. Previous studies have noted that industrial metallic wastes tend to reduce slump due to their irregular geometry, while nanomaterials intensify this effect by increasing the paste viscosity and yield stress [35,36]. Despite the reduction in slump, all mixes remained within a workable range suitable for casting, suggesting that appropriate use of superplasticizers could further mitigate workability loss without compromising mechanical performance.

3.4. Water Absorption

A clear trend in the water absorption behavior of the concrete cylindrical specimens can be observed from the results presented in Table 5. It is noted that the water absorption percentage decreases with increasing contents of SSW and GNMPs. Among all mixes, the specimen containing 100% SSW and 0.5% GNMPs exhibited the lowest water absorption, whereas the control specimen without SSW and GNMPs showed the highest value. The decrease in water absorption can mainly be attributed to two factors. Firstly, the incorporation of SSW particles leads to reduced porosity and improved packing density within the concrete matrix due to their angular shape and rough surface texture. This enhanced packing promotes a stronger bond between the SSW particles and the cement paste, resulting in a denser and more durable concrete structure. Secondly, the presence of GNMPs also contributes to the decreasing trend in water absorption, particularly at higher dosage levels. GNMPs provide additional nucleation sites for hydration products and promote the formation of a denser calcium–silicate–hydrate (C–S–H) gel, which further refines the pore structure. The combined effect of these mechanisms results in a compact and well-packed concrete matrix. A graphical representation of these results is illustrated in Figure 5.

Table 5. Summary of water absorption, dry density, and UPV results.

Sample ID	Water Absorption (%)	Dry Density (kg/m^3)	UPV (m/s)	UPV-Based Quality
G0-SSW0	2.71	2500	4.10	Good
G0.1-SSW0	2.70	2529	4.12	Good
G0.3-SSW0	2.61	2566	4.12	Good
G0.5-SSW0	2.59	2589	4.15	Good
G0-SSW50	1.96	2664	4.35	Good
G0.1-SSW50	1.98	2681	4.38	Good
G0.3-SSW50	1.92	2704	4.41	Good
G0.5-SSW50	1.87	2733	4.44	Good
G0-SSW100	1.70	2871	4.60	Excellent
G0.1-SSW100	1.69	2888	4.65	Excellent
G0.3-SSW100	1.58	2945	4.65	Excellent
G0.5-SSW100	1.22	2999	4.67	Excellent

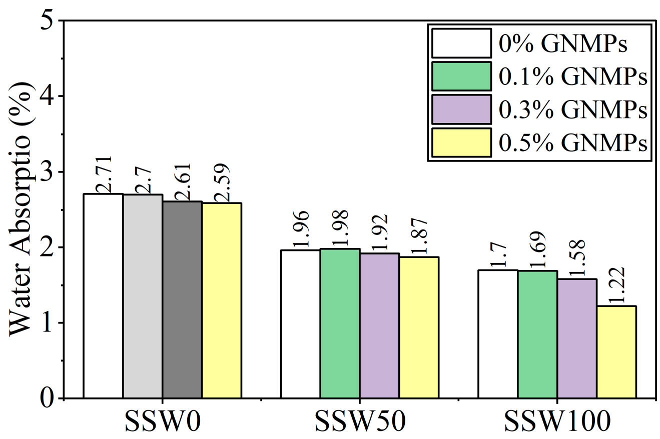

Figure 5. Water absorption of specimens.

3.5. Dry Density

The density of the hardened concrete samples was determined after 28 days of curing, and the corresponding findings are given in Figure 6 and Table 5. It was noted that both GNMPs and mill scale contributed significantly to the increase in hardened concrete density. The incorporation of GNMPs alone resulted in concrete that was denser than the control mix, with density values increasing as the GNMPs content was raised. Among all mixtures, the D-S0SSW100 mix achieved the highest density of 2999 kg/m^3, whereas the control mix A-S100SSW0 showed the lowest bulk density of 2500 kg/m^3.

The increase in density may be mainly ascribed to the filler effect of the nanoparticles, which leads to a reduction in porosity through the sealing of micro-level pores and improved contact surface area within the cementitious matrix. These findings are consistent with previously reported works that observed an enhancement in concrete density following the addition of GNMPs.

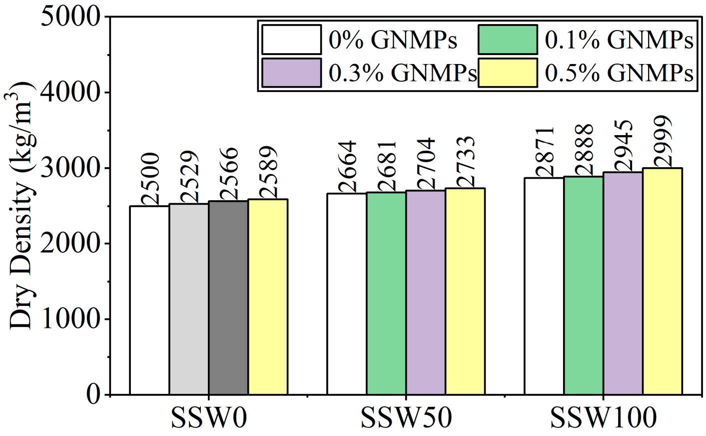

Figure 6. Dry density of specimens.

3.6. Sorptivity Test

The effect of mill scale and graphene nanoplatelets (GNMPs) on the bulk water sorptivity of concrete is examined in this work. A clear trend can be observed in Table 6, which illustrates the amount of water absorbed by the specimens over a one-day period when water ingress was allowed through only one cross-sectional surface. The results show a noticeable reduction in bulk sorptivity with the incorporation of mill scale and increasing GNMPs content, indicating a direct relationship between material addition and reduced water absorption of concrete. Sorptivity is an important durability parameter that reflects the ability of porous materials to absorb water through capillary action. A lower sorptivity coefficient indicates improved resistance to chemical penetration and environmental degradation, which ultimately enhances the durability and service life of concrete. In this test, the sorptivity coefficient was found depending on the weight gain of the samples, ascribed to water absorption of concrete through a single exposed surface. The experimental results indicate that concrete mixes containing different proportions of GNMPs and mill scale exhibited lower sorptivity values compared to the control mix. This reduction is mainly attributed to the influence of GNMPs on the transport properties of the cementitious matrix, where refinement of gel pores and improvement in microstructural density occur. These results are in accordance with previous studies, including the work of Ahmad et al. [49], which reported improved durability performance of cement-based composites incorporating GNMPs. The observed decrease in sorptivity suggests that the combined use of GNMPs and mill scale can significantly enhance the durability and overall performance of concrete. By improving the internal microstructure and limiting chemical ingress, these materials contribute to the development of more sustainable and resilient concrete systems. The detailed absorption data in terms of time and corresponding weight gain at different intervals up to 24 h are presented in Tables 6 and 7.

Table 6. Percentage absorption in terms of time passed.

Sample ID	Initial Time	1 min	3 min	5 min	15 min	30 min	60 min	24 h
G0-SSW0	0.0	0.163	0.315	0.395	0.477	0.644	1.107	1.612
G0.1-SSW0	0.0	0.204	0.289	0.372	0.422	0.548	0.643	1.038
G0.3-SSW0	0.0	0.204	0.367	0.422	0.506	0.685	0.852	1.777
G0.5-SSW0	0.0	0.204	0.309	0.410	0.543	0.757	0.949	2.196
G0-SSW50	0.0	0.390	0.488	0.488	0.585	0.683	0.780	1.463
G0.1-SSW50	0.0	0.293	0.488	0.878	1.170	1.268	1.755	2.730
G0.3-SSW50	0.0	0.293	0.390	0.390	0.488	0.585	0.683	1.170
G0.5-SSW50	0.0	0.390	0.585	0.780	0.975	1.268	1.560	2.535

Table 6. *Cont.*

Sample ID	Initial Time	1 min	3 min	5 min	15 min	30 min	60 min	24 h
G0-SSW100	0.0	0.195	0.293	0.390	0.488	0.585	0.683	1.365
G0.1-SSW100	0.0	0.293	0.390	0.488	0.585	0.780	0.878	1.658
G0.3-SSW100	0.0	0.290	0.487	0.585	0.682	0.877	0.975	1.755
G0.5-SSW100	0.0	0.290	0.487	0.585	0.682	0.780	0.877	1.560

Table 7. Percentage absorption of water in terms of water weight.

Sample ID	Initial Time	1 min	3 min	5 min	15 min	30 min	60 min	24 h
G0-SSW0	1038	1040	1041	1042	1043	1045	1049	1055
G0.1-SSW0	1092	1094	1095	1096	1097	1098	1099	1103
G0.3-SSW0	1080	1082	1083	1085	1085	1087	1089	1098
G0.5-SSW0	1093	1095	1096	1097	1098	1100	1102	1115
G0-SSW50	1226	1230	1231	1231	1232	1233	1234	1241
G0.1-SSW50	1237	1240	1242	1246	1249	1250	1255	1265
G0.3-SSW50	1159	1229	1163	1163	1164	1165	1166	1171
G0.5-SSW50	1162	1166	1168	1170	1172	1175	1178	1188
G0-SSW100	1217	1219	1220	1221	1222	1223	1224	1231
G0.1-SSW100	1300	1303	1304	1305	1306	1308	1309	1317
G0.3-SSW100	1278	1282	1283	1284	1285	1287	1288	1296
G0.5-SSW100	1264	1268	1269	1270	1271	1272	1273	1280

3.7. Ultrasonic Pulse Velocity

From a statistical point of view, the UPV results indicate the presence of a dense and well-compacted core in all the tested specimens. It is worth noting that the UPV values improved with increasing contents of GNMPs and SSW. This improvement can be attributed to the influence of GNMPs on the transport properties of the cement matrix, which enhances the microstructure and refines the gel pores. In addition, the improved bonding between SSW particles and the cement paste, due to their rough surface texture and angular shape, also contributes to the formation of a denser concrete structure. The UPV test results are presented in Table 5 and are shown graphically in Figure 7, while the UPV quality classification criteria are summarized in Table 5.

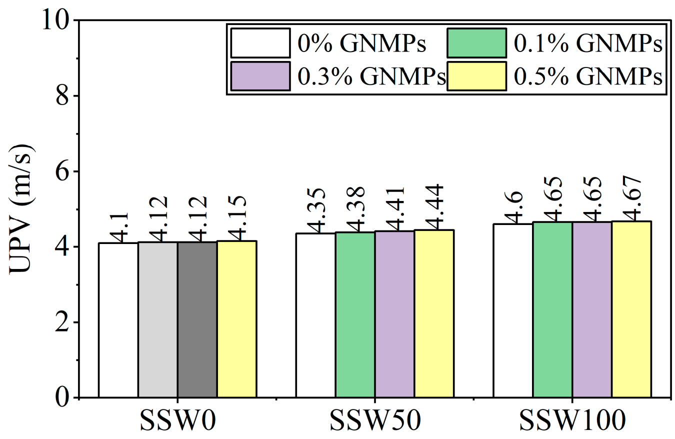

Figure 7. UPV results of specimens.

3.8. Chloride Ion Penetration

Table 8 presents the chloride ion penetration findings of the different concrete mixes, and the same results are illustrated graphically in Figure 8. It may be noted that the total charge passed reduced with increasing contents of SSW and GNMPs, indicating lower chloride ion penetrability of the concrete. This reduction can be mainly ascribed to enhanced filling and bonding within the matrix, ascribed to the combined addition of silica fume, quartz powder, SSW, and GNMPs. The presence of silica fume promotes the formation of additional hydration products, which fill the voids between aggregates, while quartz powder also contributes through its filler effect, resulting in a denser matrix. Consequently, the combined use of silica fume, quartz powder, and SSW leads to the development of a refined, dense, and compact mortar structure that offers greater resistance to chloride ingress and other aggressive liquids. Furthermore, the formation of insoluble iron carbonate compounds, such as siderite and ankerite, at later ages due to the presence of SSW contributes to pore refinement and reduced porosity, thereby lowering chloride ion penetration.

Table 8. Chloride ion penetrability.

Sample ID	Charged Pass (Coulombs)	Chloride Ion Penetrability
G0-SSW0	1770	Low
G0.1-SSW0	1722	Low
G0.3-SSW0	1697	Low
G0.5-SSW0	1700	Low
G0-SSW50	1450	Low
G0.1-SSW50	1412	Low
G0.3-SSW50	1392	Low
G0.5-SSW50	1397	Low
G0-SSW100	955	Very low
G0.1-SSW100	905	Very low
G0.3-SSW100	882	Very low
G0.5-SSW100	895	Very low

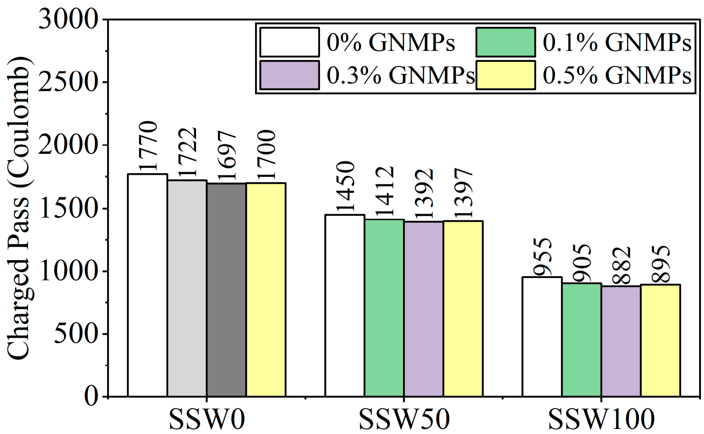

Figure 8. Charged pass for chloride ion assessment.

3.9. Discussion of Results

The present study evaluated durability-related properties primarily through water absorption and sorptivity tests, which are widely recognized as indicators of the permeability and pore structure of concrete. The observed reduction in both parameters for mixtures containing steel scale waste and GNMPs suggests the development of a denser cementitious matrix with reduced capillary pore connectivity. Such microstructural refinement generally contributes to improved resistance against environmental deterioration mechanisms, including freeze–thaw damage, sulfate attack, and chloride ingress. Although these long-term durability aspects were not directly investigated in the current experimental program, the improved permeability characteristics indicate promising durability potential of the proposed mixtures. Although microscopic characterization techniques were not conducted in the present study, the observed improvements in mechanical strength and durability-related properties can be associated with several microstructural mechanisms reported in the literature. The incorporation of GNMPs can promote the nucleation and growth of hydration products, particularly C–S–H gel, leading to a more compact cementitious matrix. Furthermore, the two-dimensional platelet structure of GNMPs may contribute to crack-bridging and restriction of microcrack propagation within the cement matrix. In addition, the use of steel scale waste as a fine aggregate replacement introduces particles with high density and angular morphology, which can improve particle packing and reduce void content. These effects collectively contribute to the refinement of the pore structure and improvement of the interfacial transition zone (ITZ) between aggregate particles and the cement paste.

To strengthen the sustainability argument, this study includes a simplified quantitative comparison: replacing natural sand with 50% SSW reduces natural sand demand by roughly 0.5 m^3 per m^3 of concrete (≈1200–1400 kg), which conservatively lowers embodied CO_2 from sand extraction/processing by about 5–10 kg CO_2-eq/m^3 (assuming 10–20 kg CO_2-eq per tonne for sand). Utilizing industrial SSW also avoids disposal emissions and reduces embodied energy by roughly 1–3 MJ/kg of substituted material, yielding an overall embodied energy reduction of ≈5–15 MJ/m^3. GNMPs are used at low dosage (0.3% by cement weight ≈ 2.1 kg/m^3 for 700 kg/m^3 cement) and add only a marginal embodied impact (on the order of <0.5 kg CO_2-eq/m^3). Net effect: the 50% SSW + 0.3% GNMP mix is estimated to cut overall embodied CO_2 by ~2–8% and embodied energy by ~3–7% versus the control, while substantially improving mechanical performance. These are order-of-magnitude estimates; a full LCA is recommended for definitive results.

4. Limitations and Future Scope

The findings of this study are based on a controlled experimental program conducted under laboratory conditions, and therefore, certain limitations should be acknowledged. The investigation focused on a limited range of steel scale waste replacement levels and graphite nano/micro platelet dosages, while other parameters such as different water-to-binder ratios, curing regimes, and aggregate gradations were not explored. Future research may extend the present work by examining a wider range of mix design parameters and incorporating long-term durability assessments under aggressive environmental exposures. The influence of alternative dispersion techniques and chemical admixtures on the performance of GNMP-modified concrete also warrants further investigation. Moreover, scaling up the proposed mixtures to structural elements and evaluating their structural behavior under flexural and shear loading would help validate the practical applicability of the findings. Life-cycle assessment and cost–benefit analysis are additionally recommended to comprehensively evaluate the sustainability potential of steel scale waste and nano-modified concrete systems.

Although the results demonstrate promising improvements in mechanical and durability-related properties, several limitations should be acknowledged. First, the mixtures investigated in this study contain relatively high cement contents typical of high-strength concrete, which may increase the risk of autogenous shrinkage and early-age cracking. The influence of SSW and GNMPs on shrinkage behavior was not evaluated in the present work and warrants further investigation. Second, while water absorption and sorptivity tests provided useful indicators of permeability, the long-term durability performance of the proposed concrete under aggressive environmental conditions—such as freeze–thaw cycles, sulfate exposure, and chloride ingress—was not directly examined. Third, the experimental program was conducted at a laboratory scale, and practical implementation in large-scale construction may present additional challenges related to material dispersion, workability control, and quality consistency during mixing and placement. Finally, further research is needed to evaluate the economic feasibility and large-scale production considerations associated with the use of graphite nano/micro platelets and industrial steel scale waste in structural concrete applications.

5. Conclusions

This study experimentally investigated the combined effects of steel scale waste (SSW) as a fine aggregate replacement and graphite nano/micro platelets (GNMPs) as a nano-modifying additive on the fresh, mechanical, and durability performance of high-strength concrete. The conclusions presented in this section are drawn directly from the results discussed in Section 3 and are limited to the observed experimental findings without extrapolation beyond the scope of the study. The key outcomes are summarized below to highlight the influence of material selection and dosage on concrete behavior.

1. The partial replacement of natural sand with SSW significantly enhanced the mechanical performance of high-strength concrete, with the 50% SSW replacement level identified as optimal. At this level, the compressive strength increased from 44.3 MPa to 57.7 MPa even without nano-modification, representing an improvement of approximately 30% compared to the control mix.
2. The incorporation of GNMPs further improved both compressive and splitting tensile strengths, with an optimum dosage of 0.3% by weight of cement consistently observed across all SSW levels.
3. Increasing the GNMP dosage beyond the optimum level resulted in a reduction in mechanical performance, particularly at 0.5% GNMPs, which is attributed to particle agglomeration and reduced dispersion efficiency within the cementitious matrix.
4. Fresh concrete workability decreased with increasing SSW content and GNMP dosage. The slump value reduced from 110 mm for the control mix to 57 mm for the mix containing 100% SSW and 0.5% GNMPs, indicating a combined effect of higher internal friction from angular SSW particles and increased water demand due to the high surface area of GNMPs.
5. Durability-related properties showed consistent improvement with the combined use of SSW and GNMPs. Water absorption and sorptivity decreased, dry density and ultrasonic pulse velocity increased, and chloride ion penetrability of concrete was significantly reduced, with very low chloride permeability achieved in mixes containing 100% SSW.

While the present study focused on the mechanical performance and fundamental durability indicators at 28 days, future investigations should examine the long-term durability behavior of SSW–GNMP modified concrete under aggressive environmental conditions, including freeze–thaw cycles, sulfate exposure, and chloride penetration, to further validate its suitability for infrastructure applications. Future research should incorporate microscopic characterization techniques such as SEM, MIP, and XRD to directly examine the pore structure distribution, hydration products, and ITZ of SSW–GNMP modified concrete.

Author Contributions: Conceptualization, S.S., M.A.B., A.N., R.F.T., S.I., P.C., C.S. and A.A.; Methodology, S.S., M.A.B., A.N., R.F.T., S.I., P.C., C.S. and A.A.; Writing—original draft, S.S., M.A.B., A.N., R.F.T., S.I., P.C., C.S. and A.A.; Writing—review & editing, Suniti Suparp, S.S., M.A.B., A.N., R.F.T., S.I., P.C., C.S. and A.A. All authors have read and agreed to the published version of the manuscript.

Funding: This research project was supported by the Faculty of Engineering, Srinakharinwirot University, Thailand (Contract Number 390/2568).

Data Availability Statement: Data are contained within the article.

Acknowledgments: This research received research funding from the Faculty of Engineering (Srinakharinwirot University, Thailand) for the fiscal year of 2025 (Contract Number 390/2568).

Conflicts of Interest: The authors declare no conflicts of interest.

References

1. Zhang, Y.; Wang, L.; Zhang, J. Evaluating the co-control potential of CO_2 and air pollutant emission reductions in the cement industry in China: A case in Henan. *J. Clean. Prod.* **2025**, *518*, 145912. [CrossRef]
2. Pejić, M.S.; Terzić, M.; Stanojević, D.; Peško, I.; Petrović, M.; Kapetina, M.; Mučenski, V. Estimating Concrete Quantities Using AI-Based Models For Recycling and Reducing CO_2 Emissions. In Proceedings of the International Scientific Conference Planning, Design, Construction and Building Renewal, Novi Sad, Serbia, 16–17 November 2023.
3. Barbhuiya, S.; Kanavaris, F.; Das, B.B.; Idrees, M. Decarbonising cement and concrete production: Strategies, challenges and pathways for sustainable development. *J. Build. Eng.* **2024**, *86*, 108861. [CrossRef]
4. Lin, L.; Wu, B. Chloride diffusion behavior of recycled lump-aggregate concrete: Experiment and numerical simulation. *Constr. Build. Mater.* **2025**, *501*, 144286. [CrossRef]
5. Lin, L.; Xu, N.; Yang, D.; Li, G.; Xiao, Y.; Yu, Y. A smart computational framework for predicting mechanical and sustainability indicators and optimizing mix proportions of recycled rubber aggregate concrete. *Eng. Appl. Artif. Intell.* **2026**, *164*, 113364. [CrossRef]
6. Saxena, S.; Baghban, M.H. Seawater concrete: A critical review and future prospects. *Dev. Built Environ.* **2023**, *16*, 100257. [CrossRef]
7. Siddique, R. *Waste Materials and By-Products in Concrete*; Springer: Berlin/Heidelberg, Germany, 2008.
8. Nawaz, A.; Khan, A.M.; Jirasakjamroonsri, A.; Saingam, P.; Ejaz, A.; Hussain, Q.; Mohamad, H.; Thansirichaisree, P. Performance of Environmentally Friendly Concrete Containing Fly-Ash and Waste Face Mask Fibers. *Sustainability* **2024**, *16*, 10385. [CrossRef]
9. Khan, Q.S.; Ahmad, R.H.; Qazi, A.U.; Kazmi, S.M.S.; Munir, M.J.; Javed, M.H. Integrated mechanical and eco-economical assessments of fly ash-based geopolymer concrete. *Buildings* **2025**, *15*, 2555. [CrossRef]
10. Shbeeb, N.I.; Akhtar, M.N. Enhancing the Sustainability of Concrete by Adding Recycled Sand and Silica Fume Along with Human Hair Fibers. *J. Compos. Sci.* **2025**, *9*, 216. [CrossRef]
11. Albadrani, M.A. Strength Development of PPC Concrete with Rice Husk Ash: Optimal Replacement Levels for Sustainable Construction. *Sustainability* **2025**, *17*, 8258. [CrossRef]
12. Lương, Q.H.; Nguy, H.H.; Choi, J.I.; Kim, H.K.; Lee, B.Y. Effects of crumb rubber particles on mechanical properties and sustainability of ultra-high-ductile slag-based composites. *Constr. Build. Mater.* **2021**, *272*, 121959. [CrossRef]
13. Zhang, X.Y.; Yu, R.; Zhang, J.J.; Shui, Z.H. A low-carbon alkali activated slag based ultra-high performance concrete (UHPC): Reaction kinetics and microstructure development. *J. Clean. Prod.* **2022**, *363*, 132416. [CrossRef]
14. Uysal, M.; Aygörmez, Y.; Canpolat, O.; Cosgun, T.; Kuranlı, Ö.F. Investigation of using waste marble powder, brick powder, ceramic powder, glass powder, and rice husk ash as eco-friendly aggregate in sustainable red mud-metakaolin based geopolymer composites. *Constr. Build. Mater.* **2022**, *361*, 129718. [CrossRef]
15. Imoh, U.U.; Habashneh, M.; Kaine, S.C.; Babafemi, A.J.; Hassan, R.; Movahedi Rad, M. Metakaolin-Enhanced Laterite Rock Aggregate Concrete: Strength Optimization and Sustainable Cement Replacement. *Buildings* **2025**, *15*, 4553. [CrossRef]
16. Kuoribo, E.; Mahmoud, H. Utilisation of waste marble dust in concrete production: A scientometric review and future research directions. *J. Clean. Prod.* **2022**, *374*, 133872. [CrossRef]
17. Das, B.; Prakash, S.; Reddy, P.S.R.; Misra, V.N. An overview of utilization of slag and sludge from steel industries. *Resour. Conserv. Recycl.* **2007**, *50*, 40–57. [CrossRef]
18. Qureshi, H.J.; Alghamdi, S.A.; Majdi, A.; Ahmad, J.; Rahmawati, C.; Alattyih, W.; Alzlfawi, A. Utilization of steel slag in concrete: A review on durability and microstructure analysis. *Rev. Adv. Mater. Sci.* **2025**, *64*, 20250086. [CrossRef]
19. Ganeshprabhu, P.; Chandrasekaran, P.; Farzana, A.S. Engineering Behaviour of Sustainable Concrete with Steel Mill Scale. *Pol. J. Environ. Stud.* **2021**, *30*, 1129–1137. [CrossRef]
20. Velumani, P.; Manikandan, P. Steel mill scale waste and granite powder waste in concrete production—An experimental study. *Mater. Today: Proc.* **2021**, *37*, 1748–1752. [CrossRef]
21. Goldmann, E.; Kudlek, E.; Bialas, O.; Górski, M.; Adamiak, M.; Klemczak, B. Environmental Toxicity of Cement Nanocomposites Reinforced with Carbon Nanotubes. *Materials* **2025**, *18*, 1176. [CrossRef]
22. Li, H.; Xiao, H.; Yuan, J.; Ou, J. Microstructure of cement mortar with nano-particles. *Compos. Part B Eng.* **2004**, *35*, 185–189. [CrossRef]
23. Alghrairi, N.; NAznieta, F.; MIbrahim, A.; Wan Hu, J.; Mohammed Najm, H.; Anas, S.M. Improvement of Concrete Characterization Using Nanomaterials: State-of-the Art. *J. Eng.* **2025**, *2025*, 8027667. [CrossRef]

24. Huang, L.; Chen, H.; Shen, J. Status and Perspectives for Mechanical Performance of Cement/Concrete Hybrids with Inorganic Carbon Materials. *Buildings* **2025**, *15*, 3525. [CrossRef]
25. Zafeiropoulou, K.; Kostagiannakopoulou, C.; Sotiriadis, G.; Kostopoulos, V. Graphene Nanofiller Type Matters: Comparative Analysis of Static and Fatigue Delamination Resistance in Modified Carbon Fiber Composites. *Polymers* **2025**, *17*, 3299. [CrossRef] [PubMed]
26. Tanyıldızı, H.; Bulut, M. The effect of carbon nanotube on self-healing properties of engineered cementitious composites subjected to high temperatures. *Struct. Concr.* **2025**, *26*, 1245–1260. [CrossRef]
27. Xi, Q.T.A.; Li, H.; Wang, S.X.; Hu, Y.G. Study of temperature and moisture effects on piezoresistive behavior of graphene oxide-reinforced cementitious composites. *J. Intell. Mater. Syst. Struct.* **2025**, *36*, 845–871. [CrossRef]
28. Akbar, A.; Liew, K.M.; Farooq, F.; Khushnood, R.A. Exploring mechanical performance of hybrid MWCNT and GNMP reinforced cementitious composites. *Constr. Build. Mater.* **2021**, *267*, 120721. [CrossRef]
29. Tufail, R.F.; Naeem, M.H.; Ahmad, J.; Waheed, H.; Majdi, A.; Farooq, D.; Maqsoom, A.; Butt, F. Evaluation of the fresh and mechanical properties of nano-engineered self compacting concrete containing graphite nano/micro platelets. *Case Stud. Constr. Mater.* **2022**, *17*, e01165. [CrossRef]
30. Iqra, 30.; Zahid, M. Impact of graphite nano/microplatelets on the mechanical and durability performance of concrete by incorporating mill scale waste. *J. Eng. Appl. Sci.* **2024**, *71*, 212. [CrossRef]
31. Zhang, M.; Li, H. Pore structure and chloride permeability of concrete containing nano-particles for pavement. *Constr. Build. Mater.* **2011**, *25*, 608–616. [CrossRef]
32. Ababneh, A.N.; Matalkah, F.; Al-Akhras, M. The use of graphene nanoplatelets for enhancement of the compressive strength of mortar containing high-levels of natural Pozzolan. *Constr. Build. Mater.* **2024**, *449*, 138302. [CrossRef]
33. Farmaki, S.G.; Dalla, P.T.; Exarchos, D.A.; Dassios, K.G.; Matikas, T.E. Thermal and Electrical Properties of Cement-Based Materials Reinforced with Nano-Inclusions. *Nanomanufacturing* **2025**, *5*, 13.
34. Le, J.-L.; Du, H.; Pang, S.D. Use of 2D Graphene Nanoplatelets (GNP) in cement composites for structural health evaluation. *Compos. Part B Eng.* **2014**, *67*, 555–563. [CrossRef]
35. Roopa, A.K.; Ambale, D.; Hunashyal, A.M.; Patil, S. Synergistic effects of cementitious nanocomposites grouts fused with epoxy coatings for restoring concrete structures. *Sci. Rep.* **2025**, *15*, 40128. [CrossRef]
36. Vincent, T.; Ozbakkaloglu, T. Influence of concrete strength and confinement method on axial compressive behavior of FRP confined high- and ultra high-strength concrete. *Compos. Part B Eng.* **2013**, *50*, 413–428. [CrossRef]
37. Amran, M.; Huang, S.S.; Onaizi, A.M.; Murali, G.; Abdelgader, H.S. Fire spalling behavior of high-strength concrete: A critical review. *Constr. Build. Mater.* **2022**, *341*, 127902. [CrossRef]
38. Shi, C.; Qian, J. High performance cementing materials from industrial slags—A review. *Resour. Conserv. Recycl.* **2000**, *29*, 195–207. [CrossRef]
39. Alkhatib, A.; Basha, S.I.; Shameem, M.; Maslehuddin, M. Use of Industrial Byproducts and Nanomaterials in Developing Sustainable Cement Concrete: A Review. *Arab. J. Sci. Eng.* **2025**. [CrossRef]
40. Lyu, K.; Qu, Y.; Liu, X.; Kou, F.; Xie, X.; Shi, J.; Liu, L.; Shah, S.P. Synergistic modification of recycled concrete powder through nano silica co-grinding: A mechanochemical approach for sustainable cementitious composites. *Constr. Build. Mater.* **2025**, *492*, 142961. [CrossRef]
41. Ali, B.; Fahad, M.; Ullah, S.; Ahmed, H.; Alyousef, R.; Deifalla, A. Development of ductile and durable high strength concrete (HSC) through interactive incorporation of coir waste and silica fume. *Materials* **2022**, *15*, 2616. [CrossRef]
42. Zhou, J.; Dong, Y.; Qiu, T.; Lv, J.; Guo, P.; Liu, X. The microstructure and modification of the interfacial transition zone in lightweight aggregate concrete: A review. *Buildings* **2025**, *15*, 2784. [CrossRef]
43. Ferreira, M.T.; Soldado, E.; Borsoi, G.; Mendes, M.P.; Flores-Colen, I. Nanomaterials applied in the construction sector: Environmental, human health, and economic indicators. *Appl. Sci.* **2023**, *13*, 12896. [CrossRef]
44. Bulińska, S.; Sujak, A.; Pyzalski, M. Sustainable management of photovoltaic waste through recycling and material use in the construction industry. *Materials* **2025**, *18*, 284. [CrossRef] [PubMed]
45. Sanchez, F.; Sobolev, K. Nanotechnology in concrete—A review. *Constr. Build. Mater.* **2010**, *24*, 2060–2071. [CrossRef]
46. Maslehuddin, M.; Sharif, A.M.; Shameem, M.; Ibrahim, M.; Barry, M.S. Comparison of properties of steel slag and crushed limestone aggregate concretes. *Constr. Build. Mater.* **2003**, *17*, 105–112. [CrossRef]
47. Qasrawi, H. The use of steel slag aggregate to enhance the mechanical properties of recycled aggregate concrete and retain the environment. *Constr. Build. Mater.* **2014**, *54*, 298–304. [CrossRef]
48. Qasrawi, H.; Shalabi, F.; Asi, I. Use of low CaO unprocessed steel slag in concrete as fine aggregate. *Constr. Build. Mater.* **2009**, *23*, 1118–1125. [CrossRef]
49. Ahmad, F.; Qureshi, M.I.; Ahmad, Z. Influence of nano graphite platelets on the behavior of concrete with E-waste plastic coarse aggregates. *Constr. Build. Mater.* **2022**, *316*, 125980. [CrossRef]
50. *ASTM C150/C150M-22*; Standard Specification for Portland Cement. ASTM International: West Conshohocken, PA, USA, 2022.

51. Huang, Y.; Chen, J.; Liu, Y. Life cycle assessment of a process integrating supercritical water gasification with direct reduced iron production. *J. Clean. Prod.* **2024**, *483*, 144250. [CrossRef]
52. Stewart, D.J.; Thomson, D.; Barron, A.R. The production of high value pig iron nuggets from steelmaking by-products—A thermodynamic evaluation. *Resour. Conserv. Recycl.* **2021**, *170*, 105592. [CrossRef]
53. *ASTM C33*; Standard Specification for Concrete Aggregates. ASTM International: West Conshohocken, PA, USA, 2018.
54. *ASTM C192/C192M-19*; Standard Practice for Making and Curing Concrete Test Specimens in the Laboratory. ASTM International: West Conshohocken, PA, USA, 2019.
55. *ASTM C39/C39M-21*; Standard Test Method for Compressive Strength of Cylindrical Concrete Specimens. ASTM International: West Conshohocken, PA, USA, 2021.
56. *ASTM C496/C496M-17*; Standard Test Method for Splitting Tensile Strength of Cylindrical Concrete Specimens. ASTM International: West Conshohocken, PA, USA, 2017.
57. *ASTM C143/C143M-20*; Standard Test Method for Slump of Hydraulic-Cement Concrete. ASTM International: West Conshohocken, PA, USA, 2015.
58. *ASTM C642-21*; Standard Test Method for Density, Absorption, and Voids in Hardened Concrete. ASTM International: West Conshohocken, PA, USA, 2021.
59. *ASTM C596-23*; Standard Test Method for Drying Shrinkage of Mortar Containing Hydraulic Cement. ASTM International: West Conshohocken, PA, USA, 2023.
60. *ASTM C1585-20*; Standard Test Method for Measurement of Rate of Absorption of Water by Hydraulic-Cement Concretes. ASTM International: West Conshohocken, PA, USA, 2020.
61. *ASTM C597-22*; Standard Test Method for Ultrasonic Pulse Velocity Through Concrete. ASTM International: West Conshohocken, PA, USA, 2022.
62. *ASTM C1202-25*; Standard Test Method for Electrical Indication of Concrete's Ability to Resist Chloride Ion Penetration. ASTM International: West Conshohocken, PA, USA, 2025.

https://doi.org/10.3390/buildings16071315